Models for Material Failure and Deformation

PAUL MEAKIN

Simple computer models have been used to investigate a variety of pattern formation processes associated with material failure and deformation. These models reproduce surprisingly well the characteristic morphologies observed in a wide range of real systems. They provide a sound basis for the development of more realistic models that can be used to develop a better understanding of the mechanical properties of real materials. The present algorithms are adequate for some purposes, but substantial improvements are needed if simulation results are to make a major contribution to our theoretical understanding of the asymptotic fractal scaling and universality properties of patterns generated by failure and deformation phenomena.

MATERIAL FAILURE AND DEFORMATION ARE OF MAJOR importance in almost all aspects of human endeavor. Consequently, they have been studied extensively for many years. Most failure and deformation phenomena of practical importance involve a variety of processes occurring on a wide range of time and length scales. Many of these are nonlinear processes occurring under nonequilibrium conditions; as such they are, in general, still quite poorly understood. Considerable effort has been devoted to the propagation of a single crack tip in a homogeneous medium, but real materials are inhomogeneous, crack geometries are often complex, and crack-crack interactions are important. In recent years, computer simulation has become a promising approach toward the development of a better understanding of cracking, forging, and drawing. Most of this work has been concerned with quite simple, even abstract, models that focus attention on those processes that are believed to be the most important for a particular system and set of conditions. The results obtained from these models provide a basis for understanding the behavior of real materials and for developing more complex and realistic models. However, even some of the most simple of these models are not at all well understood theoretically. At this stage it seems that the development of practical general models that can be applied to a wide variety of materials under a broad range of conditions is still a quite distant prospect.

Despite the complexities outlined above, there is good reason for being optimistic. The current high level of interest in nonlinear phenomena and nonequilibrium pattern formation is leading to the development of new methods and concepts that are beginning to be applied to problems such as crack growth. In some cases very similar cracking patterns are seen in a wide range of materials over a broad range of length scales. "Mud-cracking" patterns can be observed in systems as diverse as microscopic thin film deposits, paint films, and multikilometer-scale basement rocks (*1*). Very similar patterns are formed in systems covering a wide range of length scales and materials (ceramics, metals, polymers, composite materials, and so on). This similarity suggests that a case-by-case study may not be required and that simple models may provide useful results. A systematic exploration of this and other universalities is an important part of the current agenda (*2–5*). The continual rapid growth in the speed, availability, and flexibility of digital computers is also expected to contribute substantially to the growth of this area.

One general approach to the simulation of mechanical properties is to represent the material by a network of structural units (bonds, springs, beams) whose rate of failure depends on local conditions (temperature, strain, radiation, chemical environment). In some models, formation as well as failure of the elements in the network is included. In most simulations the failure or deformation process is implemented via a Monte Carlo procedure. Other approaches [notably molecular dynamics (*6–10*)] have also been successfully exploited.

Network Models

In a wide variety of models for failure and deformation, the "material" is represented by a network of mechanical elements (bonds, springs, beams) that have their own mechanical properties. These properties depend on the purpose for which the model is intended. In models that are used to represent in detail the behavior of specific materials, each element in the network may have quite complex, time-dependent properties. Here we are concerned primarily with "universal" phenomena that occur in a wide range of materials. Under these circumstances it is natural to explore simple generic models. In most of the models, the network elements can exist in two mechanical states and the kinetics of failure and deformation are controlled by the strain-dependent transition rates between these two states. In most cases one of the two states corresponds to complete failure (removal) of the network element. This process may be reversible, but in most models material failure is considered an irreversible process.

In a typical Monte Carlo simulation, an element of the network is selected at random with a probability $P(\Omega)$ that depends on the local configuration Ω. After an element has been selected, it is removed from the network (or its properties are changed), and the network is allowed to partially or completely relax to a new mechanical equilibrium (subject to appropriate mechanical boundary conditions). The new network element bond-breaking probabilities (rates) are then calculated, and the process of transition between mechanical states and relaxation is repeated many times to simulate the material failure or deformation process. Most simulations have been carried out with complete relaxation of the network. Such models are clearly more appropriate for processes such as slow crack growth, in which complete mechanical relaxation is physically

The author is at Central Research and Development, E. I. du Pont de Nemours and Company, Wilmington, DE 19880.

realistic, than for fast processes such as brittle fracture.

The rate of failure of many materials increases very rapidly with increasing stress or strain. It seems natural to suppose that this macroscopic behavior has a microscopic origin and that the failure of individual network elements also depends strongly on the local stress or strain. Consequently, models in which the failure or modification rate constant R_f is related to the local force f associated with these elements by relations such as

$$R_f \sim f^\eta \tag{1}$$

or

$$R_f \sim \exp(af^n) \tag{2}$$

have been explored. However, the assumption that the rate of failure or modification depends only on the local stress cannot be justified quantitatively and may have to be modified if an accurate simulation of the properties of real materials is required. The form given in Eq. 2 is supported by the absolute reaction rate theory for chemical processes (*11–13*). According to this theory, the rate constant of a chemical process (such as bond breaking) can be written as

$$R = b(T) \exp(-E_a/k_bT) \tag{3}$$

where E_a is the activation energy, k_b is the Boltzmann constant, T is the temperature, and $b(T)$ is a weakly temperature-dependent preexponential factor. For stress-induced failure, Eq. 3 can be written as

$$R = b(T,f) \exp(-E_a(f)/k_bT) \tag{4}$$

In most cases $E_a >> k_bT$ and the preexponential factor $b(T,f)$ can be approximated by a constant. The main effect of exerting an external force on the system is to reduce E_a by an amount that depends on f (or the local bond length displacement δ). For a simple harmonic potential the elastic energy stored in a distorted bond is given by

$$E_s = k\delta^2/2 = f^2/2k \tag{5}$$

where k is the bond force constant.

If it is assumed that E_a for bond breaking is reduced by an amount proportional to E_s, then a value of 2 is obtained for the exponent n in Eq. 2. It might also be argued that the bond has broken when δ has reached a critical value δ_0 and that the energy required to reach this displacement will be reduced by an amount proportional to f. These simple ideas are not realistic, and at this stage Eq. 2 must be regarded as an empirical relation. For polymers a considerable amount of experimental data support the idea that E_a is reduced by an amount that is proportional to the stress (σ) (*14–17*). Under these circumstances the bond-breaking rate constant can be expressed by the form

$$R = \nu_0 e^{-(E_a - \beta\sigma)/k_bT} \tag{6}$$

where ν_0 is a thermal vibration frequency. For three-dimensional systems, the parameter β in Eq. 6 can be interpreted as an activation volume. For the breaking of a bond in a network, β can be interpreted as an activation length (β') and σ can be replaced by f.

It might be inferred from the above discussion that the elements in the network should be interpreted on a molecular level. However, in most cases a more macroscopic interpretation in which the elements of the network represent physical structures such as grains, dislocations, or other extended structures seems to be more appropriate. In other cases the elements in the network may represent the material in a characteristic volume of size (length) determined by the fracture process itself [the size of the plastic zone, for example (*18, 19*)].

Random fluctuations appear to be an important ingredient in material deformation and failure processes. However, in the Monte Carlo models outlined above, randomness enters the models in a relatively uncontrolled fashion. The degree of randomness can be controlled by methods such as noise reduction in which a network element must be selected m times before it finally fails or is modified (*20–22*). Disorder can also be introduced in a quite different way. The elements in the network can be considered to be "damaged" at rates given by Eqs. 1, 2, or 6 and to fail when the damage associated with the ith element reaches a threshold value (T_i). Apart from the random distribution of threshold values that are assigned at the start of a simulation, models of this type with "quenched" disorder are completely deterministic. When the damage associated with one of the elements in the system reaches its T_i, it is removed or modified. The system is then relaxed to a new mechanical equilibrium, and new damage rates are calculated. The "damage" associated with each of the bonds is then increased at the new damage rates until the next bond reaches its damage threshold. The simulation proceeds by a sequence of damage growth, network modification, and relaxation steps until the "material" fails completely or a preselected number of network elements have been modified. In these models the disorder can be controlled via the distribution of threshold values. In many cases the introduction of disorder via random bond selection or quenched disorder (random damage thresholds) leads to very similar damage patterns and kinetic behavior. This behavior is similar to that found for the closely related diffusion-limited aggregation (DLA) model (*23*). In this case simulations carried out with the use of deterministic models with quenched disorder (*24*) lead to patterns that are similar to those obtained with the standard DLA model. The DLA model corresponds to the random selection of growth sites with probabilities given by a scalar field ϕ that obeys the Laplace equation

$$\nabla^2\phi = 0 \tag{7}$$

with absorbing boundary conditions ($\phi = 0$) on the surface of the growing pattern and a fixed value for ϕ ($\phi = 1$) at infinity. This model has been found to describe quite well both the kinetics (*25*) and the structure (*26*) of fluid-fluid displacement in a porous medium (an essentially deterministic process that takes place in a random medium with "quenched" disorder). Quenched disorder can also be introduced via a random distribution of strain, stress, or elastic energy thresholds. In models of this type the network element that most exceeds its threshold may be modified (*27*) or more complex criteria that include "memory" effects may be used (*28*).

The models outlined above can be used to investigate both the kinetics of crack growth and the morphological aspects of cracking processes. For example, a time scale can be introduced into models in which the elements of the network are selected at random. In one version of these models the elements in the network are selected randomly with equal probabilities. After an element has been selected, a random number x uniformly distributed over the range $0 < x < 1$ is generated and the selected element is modified if $x < R_i/R_{max}$ where R_i is the removal (or modification) rate constant for the selected element and R_{max} is the maximum rate constant for any element in the network. Each time an element is selected (whether or not it is modified), the time is incremented by an amount δt given by

$$\delta t = 1/NR_{max}) \tag{8}$$

where N is the number of unbroken (or unaltered) network elements. The time scale introduced in this manner is directly proportional to the real (physical) time associated with the cracking or deformation process.

If the bond-breaking frequencies are known (for example, if ν_0, E_a, and β in Eq. 6 are known), then an absolute time scale can be introduced in a similar fashion. In most cases there are substantial

uncertainties concerning both the detailed physical description of material failure processes and the parameters used in the models. Consequently, a quantitative agreement between time scales of computer models and real systems either is usually fortuitous or is a result of tuning the model parameters. Information concerning relative time scales obtained from kinetic models for mechanical behavior is generally much less sensitive to model parameters.

DLA and Related Models for Crack Growth

In the DLA process (*23*), particles are added one at a time to a growing cluster or aggregate via random walk trajectories originating from outside the region occupied by the cluster. A simple square lattice version of this model is illustrated in Fig. 1. This model leads to the formation of random fractal (*29*) patterns that closely resemble those associated with a variety of physical processes including fluid-fluid displacement processes (*24–26*), electrodeposition, dielectric breakdown, the dissolution of porous materials, and some biological growth processes [some of these applications are reviewed in (*30–32*)]. Structures covering a wide range of length scales (Fig. 2) can be generated with improved DLA algorithms (*33–35*). The DLA model is closely related to simple models for the growth of cracking patterns. Processes such as dielectric breakdown and fluid-fluid displacement are closely related to other material "failure" processes such as cracking. This is particularly evident in the work of Van Damme (*36–38*) on the displacement of clay dispersions by air or water in a Hele-Shaw cell (two parallel sheets of glass with a small constant gap that contains the fluids). At low clay concentrations the displacement patterns closely resemble those associated with the DLA model (Fig. 2). As the clay concentration is increased, a transition from a "fluid displacement" to a "cracking pattern" is observed (Fig. 3).

The close relation between DLA and material failure is also exhibited quite explicitly by the dielectric breakdown version of this model (*39*). In this model the Laplace equation (Eq. 7) is discretized to give

$$\phi_{ij} = 1/4(\phi_{i-1,j} + \phi_{i+1,j} + \phi_{i,j-1} + \phi_{i,j+1}) \quad (9)$$

and is solved numerically (with appropriate boundary conditions; see above) on a lattice to obtain the growth probabilities [in Eq. 9 the discretized Laplace equation is given for a square lattice where ϕ_{ij} is the value of the scalar harmonic field associated with the lattice site with coordinates (i,j)]. Unoccupied perimeter sites are selected randomly with probabilities that are given by

$$P(i,j) \sim \phi(i,j)^{\eta} \quad (10)$$

or

$$P(i,j) \sim n\phi(i,j)^{\eta} \quad (11)$$

and filled to represent the growth process. In Eq. 11, n is the number of filled sites adjacent to the unoccupied perimeter site. The simple homogeneous (power law) relation between the growth probabilities (P) and the scalar field (ϕ) in Eqs. 10 and 11 is motivated primarily by theoretical considerations. A simple homogeneous relation between P and ϕ is expected to generate patterns with relatively simple fractal scaling properties, whereas more inhomogeneous complex relations between P and ϕ will lead to structures with more complex geometric scaling behavior. For the case $\eta = 1$, this model generates random patterns that are very similar to those associated with the DLA model. Because the harmonic field (ϕ) must be relaxed after each growth event, this model cannot be used to generate very large clusters such as that shown in Fig. 2.

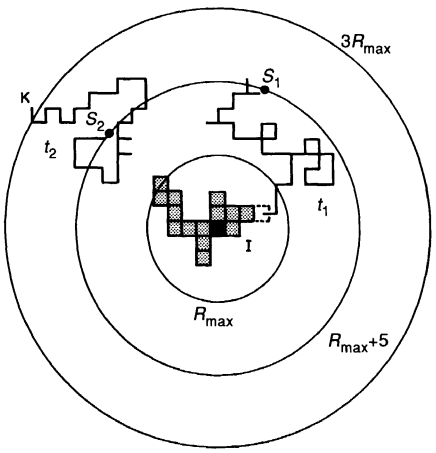

Fig. 1. An early stage in a square lattice model simulation of diffusion-limited aggregation. The original seed or growth site is shown in black, and the other sites that are occupied at this stage are shaded. Two typical trajectories starting at random positions on the launching circle (a circle that just encloses the growing cluster) are shown. Trajectory t_1 reaches an unoccupied surface site (growth site) that is indicated by-dashed edges, and this site is occupied. Trajectory t_2 reaches the termination circle, which in this case has a radius of $3R_{max}$, where R_{max} is the maximum radius of the cluster. This trajectory will be terminated and a new trajectory started at a random position on the launching circle. S_1 and S_2, starting positions; I, initial growth site; K, terminal site.

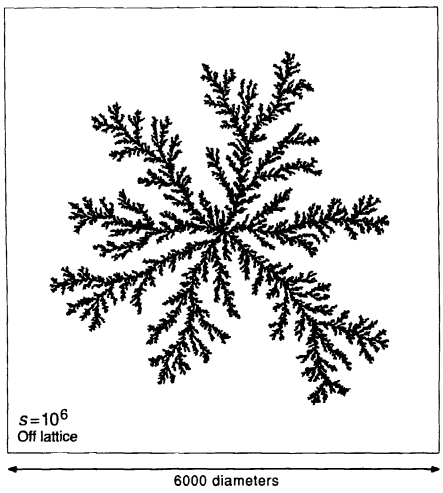

Fig. 2. A cluster of 10^6 particles generated using a two-dimensional off-lattice model for diffusion-limited aggregation.

The DLA model provides a basis for understanding a broad range of phenomena such as those mentioned above. Despite its apparent simplicity, our theoretical understanding of this model is still far from complete and it is now regarded as a major theoretical challenge. The success of the DLA model and the intense interest that it has generated have stimulated the development of a broad range of models for the formation of disorderly patterns under nonequilibrium conditions (*31, 40, 41*). In view of the results obtained with the dielectric breakdown version of the DLA model, it is natural to think of simulating mechanical breakdown processes by means of a similar model. In the most simple case we are concerned with a crack propagation process controlled by a displacement field $\mathbf{U}$ that obeys the Navier equation (*42*)

$$(\lambda + \mu)\nabla[\nabla \cdot \mathbf{U}] + \mu\nabla^2\mathbf{U} = 0 \quad (12)$$

for linear elasticity where the quantities λ and μ are the Lamé coefficients (*43*).

The first successful model of this type was developed by Louis and Guinea (*44–46*). A triangular lattice is used to represent the elastic medium rather than a square lattice because a square network of nodes with nearest neighbor central force interactions would have no shear modulus. In these DLA-like models it is assumed that only those bonds on the surface of the crack (which is initiated by removing a bond near the center of the network) are broken as the crack grows. There are several different ways in which the surface

Fig. 3. Transition from viscous fingering to cracking patterns. These patterns were generated by injecting water into aqueous bentonite clay suspensions or pastes in a pseudo two-dimensional radial cell. The clay particle concentration (w/w) increases from 0.08 in the left pattern, 0.10 in the middle pattern, and 0.20 in the right pattern. As the concentration increases, the branching angle increases and the morphology of the pattern becomes more fracture-like. [Figure provided by H. Van Damme, CNRS, Orleans, France]

bonds can be defined. Three of these possibilities will be referred to as model I, model II, and model III, respectively. In model I only those bonds joining pairs of nodes that are both on the crack perimeter can be broken. In model II any bond associated with a damaged node (a node with five or fewer bonds) can be broken, and in model III any of the bonds associated with any of the nodes at the crack perimeter can be broken. Model II was used in the original work of Louis *et al.* (*44, 45*).

In this model the bond-breaking probabilities P_i are given by

$$P_i = \delta_i^{\eta} / \sum_{j=1}^{N} \delta_j^{\eta} \tag{13}$$

where $\delta_i = \ell_i - \ell_0$ is the bond strain (ℓ_i is the bond length and ℓ_0 is the equilibrium bond length) and N is the number of surface bonds. In most simulations the network is dilated isotropically (by a small amount to avoid unwanted nonlinearities), and the positions of the nodes at the edges of the network are fixed. In some cases, a constant force is applied to the nodes at the perimeter of the network. Figure 4 shows the results of simulations carried out with all three models for the local boundary conditions at the crack surface with a growth probability exponent (η) of 1. The patterns generated by these models are quite similar to those associated with the DLA model. These patterns are probably asymptotically self-similar fractals, and their fractal scaling properties can be measured with the methods that have been applied to DLA. Unfortunately, the amount of computer time required to grow a cracking pattern consisting of a few thousand broken bonds is comparable to that required to grow a DLA cluster with a few million sites or particles. The dependence of the radius of gyration (R_g) of the simulated cracking patterns on the number of broken bonds (s) can be represented quite well by the algebraic relation

$$R_g \sim s^{\beta} \tag{14}$$

for patterns containing more than a few tens of broken bonds, but the accessible power law regime spans less than an order of magnitude in length scales. The values obtained for the fractal dimensionality ($D_\beta = 1/\beta$) from Eq. 14 are given in Table 1 (*47*).

Simulations have also been carried out with similar models with shear strain (*45–49*) or uniaxial extension (*48, 49*). With shear strain the cracking pattern has an x-like shape (if only bonds in tension are allowed to break, only one arm of the x shape grows) for model I, II, and III boundary conditions and for different orientations of the shear with respect to the lattice axes. Effective values for D_β obtained via Eq. 14 are shown in Table 1 for some of these shear models. Hinrichsen *et al.* (*48*) have obtained very similar cracking patterns using essentially the same model. However, they analyzed their cracking patterns differently and concluded that the fractal dimensionality for model I is 1.28 ± 0.06 (substantially lower than the value shown in Table 1). They pointed out that the individual arms of the racking patterns generated using shear strain are very similar to the patterns generated using uniaxial compression (or tension). This suggests that the patterns may be self-affine (*50*). It seems quite possible that the asymptotic global fractal dimensionality (*50*) may be 1.0. This example illustrates the practical difficulties that are encountered when fractal geometry is used to characterize such small structures.

Table 1. Effective fractal dimensionalities (D_{eff}) obtained from the DLA-like crack growth models. The effective fractal dimensionalities were obtained by least-squares fitting straight lines to the coordinates [log(R_g), log(s)] for the larger values of s. Because of both finite size effects and statistical uncertainties, the values of D_β given here may not be close to their asymptotic values. Particularly for model III, the simulated clusters exhibit geometric scaling over only a small range of length scales.

Growth exponent (η)	Stress field	Surface model	D_{eff}
1	Dilation	I	1.35
1	Dilation	II	1.51
1	Dilation	III	1.66
1	Shear	I	1.42
1	Shear	II	1.62
1	Shear	III	1.65
2	Dilation	I	1.12
2	Dilation	II	1.16
2	Dilation	III	1.45
2	Shear	I	1.17
2	Shear	II	1.49
2	Shear	III	1.40

Surface Cracking Models

A model for surface cracking (*51*) can be constructed from a triangular network of Hookean bonds with central force interactions. For this system the elastic energy is given by

$$E = 1/2 \sum_{ij} k_{ij} (\ell_{ij} - \ell_0)^2 \tag{15}$$

where ℓ_{ij} is the distance between the ith and jth nodes and k_{ij} is the corresponding force constant. Here $k_{ij} = k$ if the nodes are connected and $k_{ij} = 0$ if the bond between the ith and jth nodes is broken. In addition, each node in the network is attached to the (rigid) substrate by a weak bond. The force exerted by this weak bond on the ith node is given by

$$\mathbf{f} = k_2 (\mathbf{r}_i^0 - \mathbf{r}_i) \tag{16}$$

where $\mathbf{r}_i$ is the position in the ith node and $\mathbf{r}_i^0$ is the position of attachment to the substrate (its position at the start of the simulation). In this model only the high modulus bonds in the surface layer are allowed to break (all the nodes remain attached to the substrate). The bond-breaking probabilities are given by

$$P_i \sim R_i = \exp(k\delta_i^2/2) \tag{17}$$

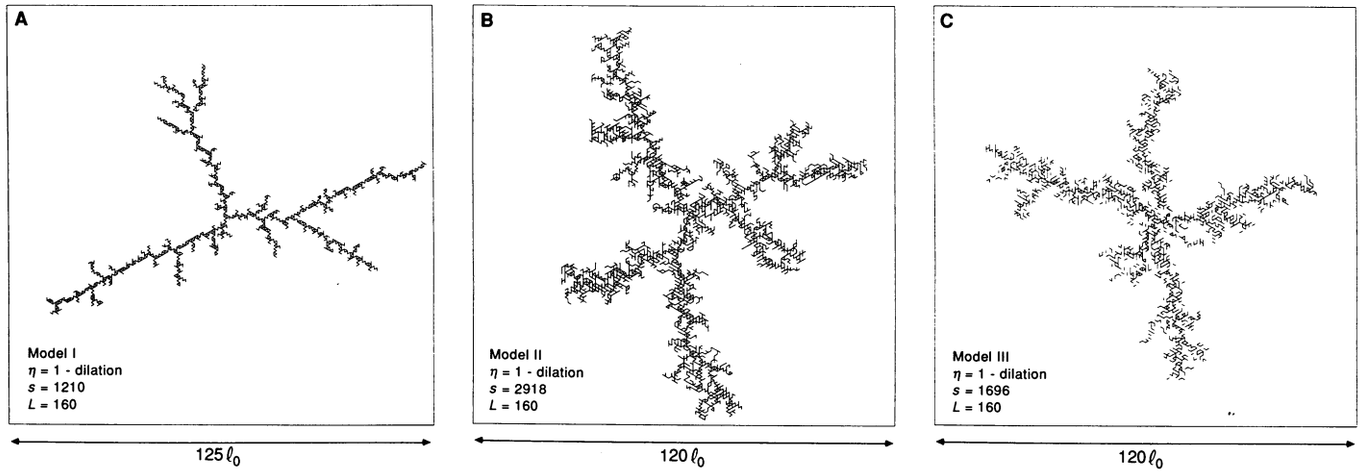

Fig. 4. Examples of cracking patterns generated with the use of the DLA-like cracking model and a bond-breaking probability exponent (η) of 1. (**A**, **B**, and **C**) Cracks generated using models in which the bonds capable of breaking correspond to models I, II, and III, respectively. [Adapted from (*47*) with permission of IOP Publishing, copyright 1989]

(Eq. 2 with a value of 2 for the exponent n). The simulation proceeds via a sequence of bond-breaking and relaxation steps.

Figure 5 shows some of the results obtained from a small-scale simulation carried out with the use of this model with the parameter $k = 800, k_2 = 8$, and an initial bond extension of 10% ($\ell = 1.0$ for all bonds in the surface layer at the start of the simulation and $\ell_0 = 0.909090\ldots$). These are typical parameters for this model. Periodic boundary conditions were used in all of the simulations. The green-blue-red-white color scale used in Fig. 5 indicates the stress (or strain) associated with each of the bonds in the surface layer. Figure 5A shows the system after 200 bonds out of the initial total of 7500 bonds (a network of 50 × 50 nodes) have been broken. This figure illustrates the stress concentration at the growing crack tips, the formation of a "shear band" (upper central region), and relaxation of much of the initial strain near to the cracks. Figure 5B shows the system after 400 bonds have broken. At this stage several "shear bands" have formed and a quite complex stress-strain field is evolving. The shear bands often appear ahead of growing crack tips and represent regions in which localized damage has occurred without complete failure of the network. Figure 5C shows a still later stage (600 broken bonds). At this stage a large fraction of the initial strain energy has been released. Results have also been obtained from much larger scale simulations with networks of 200 × 200 nodes joined by 120,000 bonds. For large values of k, the first cracks to be formed are quite linear; but, as the cracking process continues, the cracks become more and more irregular.

These simulations can easily be made time-dependent by use of the approach outlined above (Eq. 8). Figure 6 shows some results from these time-dependent simulations (for dilational strain in the surface layer at the start of the simulations). These and other simulations indicate the following scenario for large values of k and $k/k_2 >> 1$. Initially isolated defects are formed, and the rate of bond-breaking is relatively slow. However, the stresses associated with bonds near these defects are larger than those farther from defects, and they have a relatively high probability of breaking. As the defects grow larger, these stress concentration effects become more important, and once a crack has developed it grows very quickly. The fast growth of the first few cracks reduces the stress in the surface film and the rate of bond-breaking becomes slower and slower as more of the elastic energy in the film is released. As the stress is progressively released, the cracks become less linear because of the reduced effects of stress concentration of the growing crack tips. These qualitative features are not very sensitive to model details. Very similar cracking patterns and kinetic behavior can be obtained with models in which the bond-breaking rates are given by

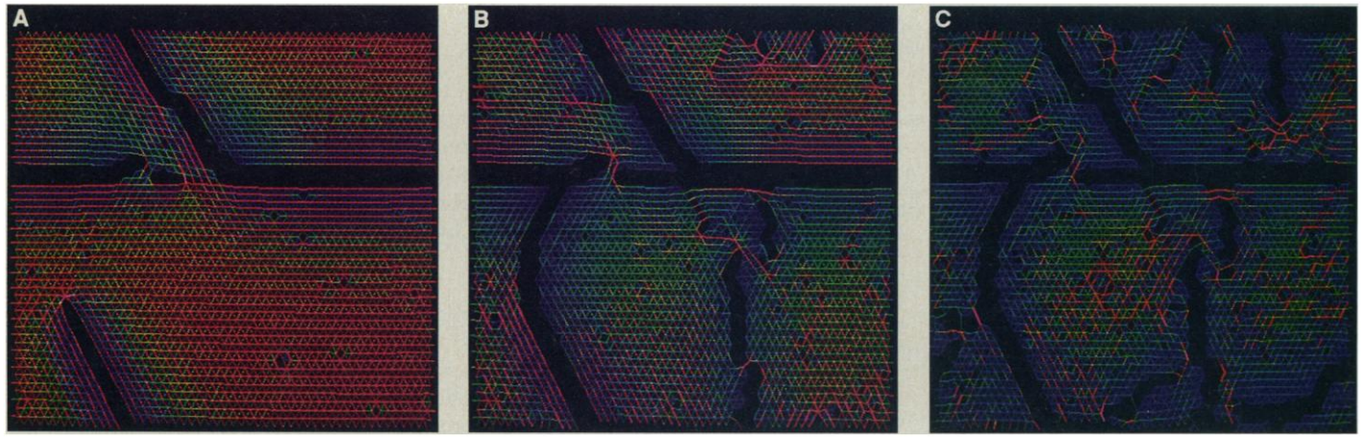

Fig. 5. Three stages in a small-scale (2500-node) simulation carried out with the surface cracking model. The green (lowest strain)-blue-red-white (highest strain) color scale illustrates the distribution of stress and strain in the surface layer.

Eq. 1 (with large values for η) or Eq. 2 with a range of values for the exponent n. In this model the randomness is controlled via the force constants k and k_2. Increasing k and k_2 together is equivalent to decreasing the temperature, because reduced units ($k_bT = 1$) are used.

Very similar cracking patterns have also been obtained from a deterministic surface cracking model with quenched disorder. In these simulations the damage threshold T_i for the ith bond is given by

$$T_i = x_i^{\theta} \tag{18}$$

where x_i is a random number uniformly distributed over the range $0 < x < 1$. In this model the disorder is controlled by the exponent θ in Eq. 18 or the force constants (temperature). This is not a very realistic threshold distribution, but the simulations indicate that very similar results can be obtained with the Monte Carlo model described above and with a corresponding deterministic model with quenched disorder.

The relaxation algorithm used in connection with this work causes the stress and strain fields to approach equilibrium via a "diffusion" process. Consequently, the number of relaxation steps required for the influence of a newly created defect to propagate through the entire system is on the order of $L^2(10^4$ to $10^5)$, where L is the size of the system. Because the total number of relaxation steps in a typical simulation also lies in the range of 10^4 to 10^5, it might seem surprising that these simulations succeed at all. However, the "weak" bonding between the surface layer and the substrate strongly localizes the effects of the crack on the stress field (the effect of the crack on the stress field decays exponentially with increasing distance from the crack). The decay length for the decay of the perturbation of an infinitely long linear crack is given by $C(k/k_2)^{1/2}$, where C is a coefficient of order unity. Without this localization, use of overrelaxation and block-relaxation (to increase the "diffusion coefficient"), and the extra relaxation cycles in the vicinity of the last broken bond, the simulations described above would not succeed.

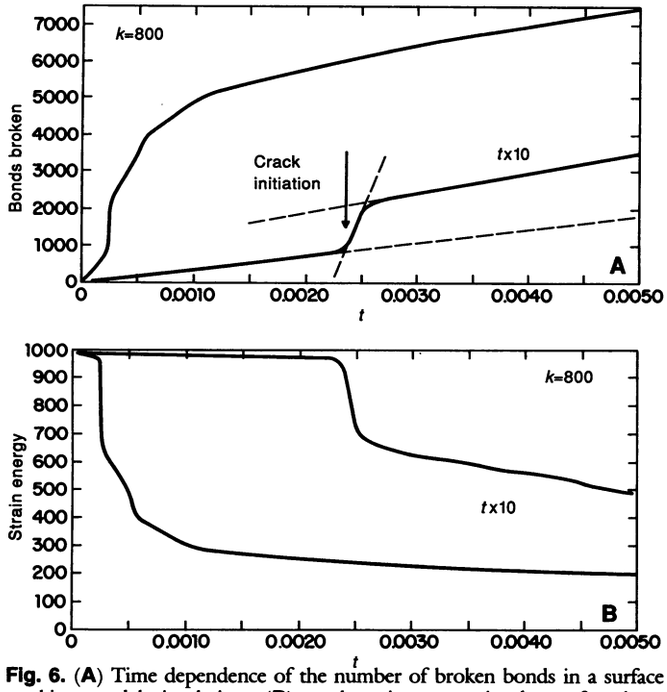

Fig. 6. (**A**) Time dependence of the number of broken bonds in a surface cracking model simulation; (**B**) total strain energy in the surface layer obtained from simulations similar to those illustrated in Fig. 5 with a value of 800 for k and 8 for k_2. These figures indicate a slow initiation period in which little strain energy is released and only isolated defects are formed, followed by a period of rapid crack propagation in which about 30% of the energy is released. This rapid release of the stress in the surface layer slows down subsequent crack initiation and propagation events. As more cracking occurs, the stress becomes still smaller and further slowing down is observed. [Adapted from (*51*) with permission of Elsevier Sequoia, copyright 1987]

Analog Simulations and Experiments

During the past 20 to 30 years, the use of computer simulations to study pattern formation processes has grown rapidly with the increased power and availability of digital computers. In a computer simulation, we can control precisely the interactions between particles, and their positions are known accurately at all times. However, even with the most advanced computers available today, most simulations are restricted to a comparatively small number of particles (typically a few hundred to a few hundred thousand) and relatively short times. The use of analog devices to explore the organization of particles under both equilibrium and nonequilibrium conditions has a long history. In recent years this approach has fallen into disfavor because of the difficulty of constructing and controlling such devices in a precise manner and because of the difficulty of obtaining quantitative results from them. In many instances, large numbers of uniformly sized and shaped particles are required to construct simple experimental models. The unavailabil-

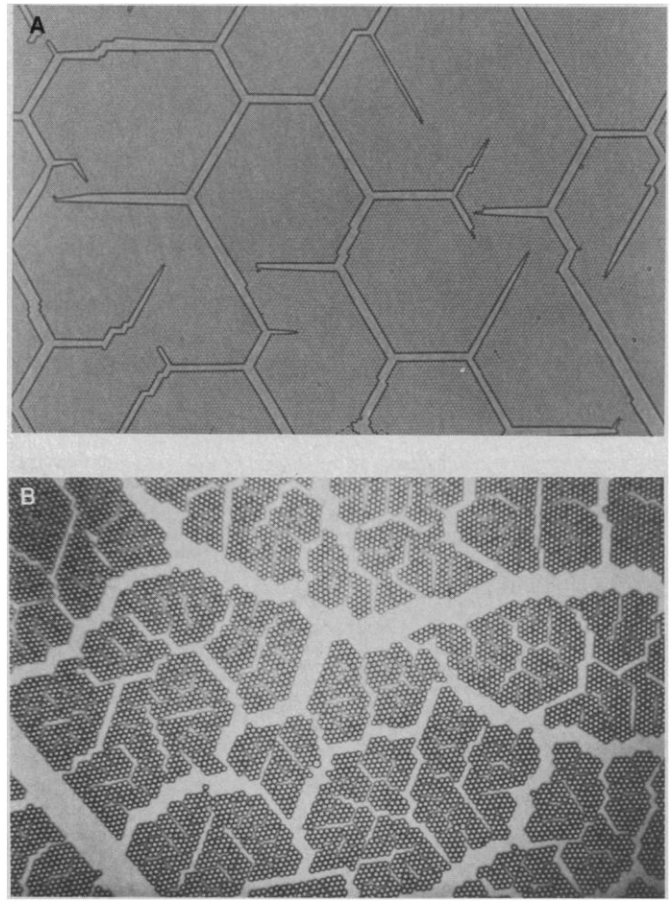

Fig. 7. Cracking inside a single grain of a sulfonated polystyrene microsphere monolayer. (**A**) The almost linear cracks that are produced at high strain in the earliest stages of cracking; (**B**) the more irregular cracking pattern that is generated under lower strain conditions later in the cracking process. [Figures provided by A. T. Skjeltorp, Institute for Energy Technology, Kjeller, Norway. (B) is reprinted from (*57*) with permission]

ity of such monodisperse particles in a suitable size range has proven to be an important obstacle to many analog experiments. The recent availability of uniformly sized polystyrene microspheres with diameters in the range 1 to 10 μm (*52, 53*) has led to the construction of experimental models for a variety of equilibrium and nonequilibrium processes (*54–56*). Microspheres in this size range can be used to construct models containing large numbers ($>10^7$) of particles, and the resulting structures can be studied by optical microscopy.

Cracking processes similar to those described in the previous section have been simulated by using an analog model consisting of a monolayer of sulfonated polystyrene microspheres with a diameter of 3.4 μm (±1%) (*57*). The initial monolayer is formed between two parallel glass sheets separated by a small number of slightly larger microspheres. The initial monolayer consists of large, almost perfectly regular regions separated by grain boundaries. The microspheres were dispersed in water to produce the monolayer, and a strained film was produced by allowing the monolayer to slowly dry. During the drying process, the sphere diameter is reduced to 2.7 μm. At first, cracking occurs along the grain boundaries; but, because of the interactions between the microspheres and the glass surfaces, the individual grains are still under substantial strain after the grain boundaries have failed. At the first stages of failure within the individual grains, small (localized) defects are formed at a relatively slow rate. This stage is followed by the rapid growth of more or less linear cracks (Fig. 7A). In the later stages, the crack growth process becomes slower and the cracks become less and less linear as the stress in the monolayer is released by the cracking process (Fig. 7B). Figure 7 shows cracking patterns generated within an individual grain.

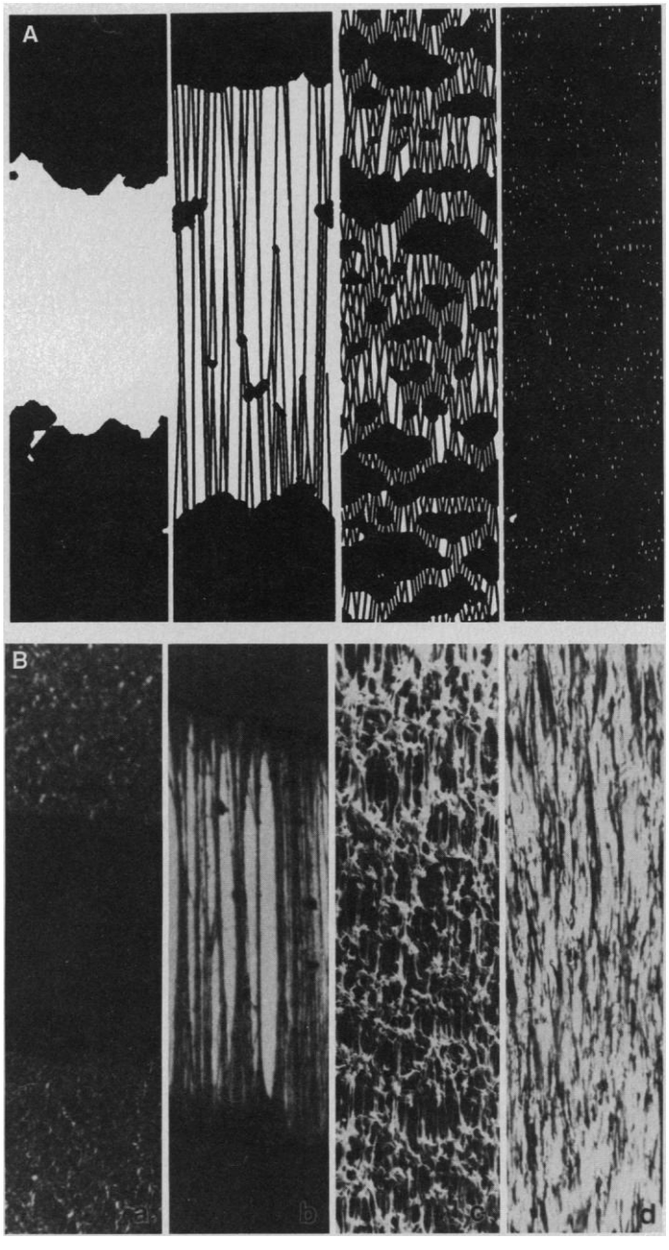

Models for Polymer Failure and Deformation

The models described above were motivated primarily by a desire to obtain a better understanding of pattern formation processes (crack growth) under nonequilibrium conditions. Another important motivation for such models is to develop a better understanding of the mechanical properties of real materials. Models developed for this purpose are in most cases (necessarily) more complex than those described above. The use of mechanical network models to describe the properties of polymer systems has a relatively long history, and applications in this direction will be used here to illustrate applications in materials science.

A serious attempt has been made to compare the simulation results with experiments on corresponding polymer systems. This is illustrated in Fig. 8 for a model that simulates failure and deformation in an entangled polymer network on the assumption that chain slippage through entanglements and the effect of weak van der Waals interactions on polymer motion play the dominant role in tensile deformation (*58*). In this model both the rate of failure of van der Waals "bonds" and the rate of chain slippage are given by Eq. 6 with different values for E_a and β. For the chain slippage process, the parameter σ in Eq. 6 represents the stress difference between two parts of a chain separated by an entanglement point.

At the start of a simulation, the system consists of a two-dimensional "diamond" lattice of nodes representing the entanglement points between pairs of polymer molecules. The lattice is then decorated randomly with polymer molecules that intersect only at the nodes (entanglement points) so that there is an entanglement point associated with every node (*58, 59*). The stress σ in the portions of the polymer chains separating entanglement points is given by the classical theory of rubber elasticity (*60*)

$$\sigma = \alpha k_b T \mathcal{L}^{-1}(r/n\ell) \quad (19)$$

Here n is the number of statistical chain segments of length ℓ between a pair of entanglement points separated by a distance r and $\mathcal{L}^{-1}$ is the inverse Langevin function $\{\mathcal{L}(x) = [\coth(x) - 1/x]\}$. The parameter α is given by (*60*)

Fig. 8. A comparison of simulated and experimental morphologies for the deformation and failure of an entangled polymer. (**A**) The simulated morphologies for four different values of the entanglement parameter $\phi = 1900/M_0$ ($\phi = 0.004$, 0.02, 0.1, and 1.0 from left to right) for simulations carried out using parameters corresponding to polyethylene. The corresponding "sample" widths were 3.2, 1.6, 0.7, and 0.2 μm, respectively. For those samples that have not failed completely, the draw ratio (λ) is 2.7. (**B**) Micrographs of drawn samples of polyethylene films of $M_w = 1.5 \times 10^6$ and $M_n \sim 2 \times 10^5$ crystallized from solutions in decalin and from the melt. These samples were drawn to a macroscopic draw ratio of approximately 3 at 100°C. The initial polymer volume fractions (φ) were 0.005, 0.02, 0.1, and 1.0 from left to right. [Figures provided by Y. Termonia, E. I. du Pont de Nemours and Company, and reprinted from (*58*) with permission of the American Chemical Society, copyright 1988]

$$\alpha = (N/3)n^{1/2} \quad (20)$$

where N is the number of chain strands per unit volume.

Like the other models discussed here, the simulation consists of a sequence of bond-breaking and relaxation steps. At frequent intervals the network is also strained along the y axis. In this model only displacements in the y direction are calculated explicitly. The coordinates in the x direction are assumed to be reduced uniformly by $\lambda^{-1/2}$, where λ is the draw ratio and periodic boundary conditions are used in the x direction. Perhaps the most drastic assumption made in this model is that, once van der Waals bonds have been broken, they are not allowed to reform. A discussion of the selection of parameters (activation energies, activation volumes, and so on) and their justification is beyond the scope of this general survey. However, two important parameters are the molecular weight M_0 between entanglement points and the polymer molecular weight (M). Figure 8A shows the results of simulations carried out for a monodisperse high molecular weight material (corresponding to M = 475,000 for polyethylene) with several different values of M_0. This quantity is expressed in terms of the ratio ϕ given by

$$\phi = 1900/M_0 \quad (21)$$

where 1900 is the value for M_0 in a polyethylene melt. For very small values of ϕ ($M = M_0$), stress concentration resulting from failure of the van der Waals bonds is not distributed by chain entanglements. Consequently, failure is highly localized and occurs at quite small strains. Figure 8B shows the results of experimental studies of the drawing of polyethylene films. The films were prepared by solidification from the melt ($M_0 \simeq 1900$) and from decalin solutions for molecular weights of $M_n = 2 \times 10^5$ and $M_w = 1.5 \times 10^6$, respectively, where M_n is the number-average molecular weight and M_w is the weight-average molecular weight. The qualitative agreement between Fig. 8, A and B, is quite striking. A more quantitative comparison between these simulations and experiments is described in (*58*).

Summary

Very large amounts of computer time on large machines (mainframe computers and supercomputers) were required to obtain the results discussed in this review. Even for the most simple cracking models it is difficult to obtain quantitative results without significant uncertainties resulting from both statistical and finite size effects. It is unlikely that the computer resources available for this type of work will improve sufficiently during the next 5 to 10 years to substantially improve this situation. Most of the simulations described above were carried out with a combination of overrelaxation and block relaxation. In some cases, techniques such as conjugate gradient (*61*) methods and Fourier acceleration (*62*) may offer substantial improvements. In practice, however, these approaches do not appear to result in significant improvements for most models. There is a clear need for improved algorithms that will allow us to grow larger structures more quickly without compromising the accuracy of the simulations. The largest cracking patterns that have been grown with current algorithms contain just a few thousand broken bonds. This contrasts with the simulations of DLA patterns for which clusters containing more than 10^7 sites have been generated in two dimensions. In addition, almost no approximations were made in the DLA simulations.

At present, there are very few results from three-dimensional simulations [apart from the rather small-scale simulations carried out more than 15 years ago by Dobrodumov and El'yashevich (*63*)]. It should not be exceptionally more difficult to carry out three-dimensional than two-dimensional simulations, and it is surprising that more work has not been done in this direction. In all of the models that have been discussed here, the material is represented by a network of nodes and bonds. These basic elements in the models do not necessarily represent structural units in real systems.

The simple models described here do not represent at all well the rich phenomenology found in most real fracture processes. They do, however, provide a firm foundation for the development of more realistic models, and this is an active area of research at the present time. For example, the models of Termonia and co-workers for polymer systems (*58, 59, 64–66*) include effects such as bond formation as well as bond breaking, finite molecular weight effects, entanglements, and orientation effects. These are fully time-dependent models that can be used to investigate the effects of strain rates and load cycling on mechanical systems. The temperature dependence of failure processes can also be explored with these models. Efforts in this direction will probably grow rapidly during the next few years. It would not unduly complicate these models to add processes such as heat generation and transport, the diffusion of low molecular weight substances, and damage by light and other radiation to these models.

The "universal" scaling behavior found by de Arcangelis *et al.* (*4*) is also an important advance. It seems probable that additional work will be carried out to delineate the range of this universality. If similar scaling behavior is found for more realistic models, this will stimulate a search for scaling and universality in experimental systems (such experiments would be worthwhile in any event). The search for universality in fracture will be slowed by the lack of efficient algorithms. This will become an even more severe problem as more complex and more realistic models are explored in this way. Even with the most simple models it is difficult to obtain unambiguous results.

REFERENCES AND NOTES

1. G. Korvin, in *Fractals in Geophysics*, C. H. Scholz and B. B. Mandelbrot, Eds. (Birkhauser Verlag, Basel, Switzerland, 1989), p. 289.
2. H. J. Herrmann and S. Roux, Eds., *Statistical Models for the Fracture of Disordered Media* (North-Holland, Amsterdam, 1990).
3. A. Hansen, S. Roux, H. J. Herrmann, *J. Phys. (Paris)* **50**, 733 (1989).
4. L. de Arcangelis, A. Hansen, H. J. Herrmann, S. Roux, *Phys. Rev. B* **40**, 877 (1989).
5. D. Sornette, *J. Phys. (Paris)* **50**, 745 (1989).
6. A. Paskin, A. Gohar, G. J. Dienes, *Phys. Rev. Lett.* **44**, 940 (1980).
7. T. F. Soules and R. F. Busbey, *J. Chem. Phys.* **78**, 6307 (1983).
8. B. K. Chakrabarti, D. Chowdhury, D. Stauffer, *Z. Phys. Sect. B* **62**, 343 (1986).
9. D. Greenspan, *J. Phys. Chem. Solids* **50**, 1245 (1989).
10. B. L. Holian, *Phys. Rev. Lett.* **36**, 3943 (1987).
11. H. Eyring, *J. Chem. Phys.* **3**, 107 (1935).
12. W. F. K. Wynne-Jones and H. Eyring, *ibid.*, p. 492.
13. S. Glastone, K. Laidler, H. Eyring, *Theory of Rate Processes* (McGraw-Hill, New York, 1959).
14. A. J. Kinloch and R. J. Young, *Fracture Behavior of Polymers* (Applied Science, London, 1983).
15. H. H. Kausch, *Polymer Fracture* (Springer-Verlag, Berlin, 1987).
16. S. N. Zhurkov and E. E. Tomashevsky, in *Proceedings of the Conference on the Physical Basis of Yield and Fracture* (Institute of Physics, 1966), p. 200.
17. S. N. Zhurkov, V. S. Kuksenko, A. I. Stutsker, in *Proceedings of the Second International Conference on Fracture* (Chapman and Hall, London, 1969), p. 531.
18. R. O. Ritchie, W. W. Geberich, J. H. Underwood, *Encyclopedia of Physical Science and Technology* (Academic Press, New York, 1987), vol. 5, p. 594.
19. D. S. Dugdale, *J. Mech. Phys. Solids* **8**, 100 (1960).
20. C. Tang, *Phys. Rev. A* **31**, 1977 (1986).
21. J. Kertesz and T. Vicsek, *J. Phys. A* **19**, L257 (1986).
22. J. Nittmann and H. E. Stanley, *Nature* **321**, 663 (1986).
23. T. A. Witten and L. M. Sander, *Phys. Rev. Lett.* **47**, 1400 (1981).
24. J. D. Chen and D. Wilkinson, *ibid.* **55**, 1892 (1985).
25. K. J. Maloy, F. Boger, J. Feder, T. Jossang, P. Meakin, *Phys. Rev. A* **36**, 318 (1987).
26. K. J. Maloy, J. Feder, T. Jossang, *Phys. Rev. Lett.* **55**, 2688 (1985).
27. W. A. Curtin and H. Sher, *J. Mater. Res.* **5**, 535 (1990).
28. H. J. Herrmann, J. Kertesz, L. de Arcangelis, *Europhys. Lett.* **10**, 147 (1989).
29. B. B. Mandelbrot, *The Fractal Geometry of Nature* (Freeman, New York, 1982).
30. R. C. Ball, in *On Growth and Form: Fractal and Non-Fractal Patterns in Physics*, H. E. Stanley and N. Ostrowsky, Ed. (NATO Advanced Study Institutes Series E100,

Nijhoff, Dordrecht, 1986), p. 69.
31. P. Meakin, in *Phase Transitions and Critical Phenomena*, C. Domb and J. L. Lebowitz, Eds. (Academic Press, New York, 1989), vol. 12, p. 335.
32. M. Matsushita, in *The Fractal Approach to Heterogeneous Chemistry: Surfaces, Colloids, Polymers*, D. Avnir, Ed. (Wiley, Chichester, U.K., 1989), p. 161.
33. P. Meakin, *J. Phys. A* **18**, L661 (1985).
34. R. C. Ball and R. M. Brady, *ibid.*, p. L809.
35. S. Tolman and P. Meakin, *Phys. Rev. A* **40**, 428 (1989).
36. H. Van Damme, in *The Fractal Approach to Heterogeneous Chemistry: Surfaces, Colloids and Polymers*, D. Avnir, Ed. (Wiley, Chichester, U.K., 1989). p. 199.
37. _____, C. Laroche, L. Gatineau, P. Levitz, *J. Phys. (Paris)* **48**, 1121 (1987).
38. H. Van Damme, F. Obrecht, P. Levitz, L. Gatineau, C. Laroche, *Nature* **320**, 731 (1986).
39. L. Niemeyer, L. Pietronero, H. J. Weismann, *Phys. Rev. Lett.* **52**, 1033 (1984).
40. T. Vicsek, *Fractal Aggregates* (World Scientific, Singapore, 1989).
41. J. Feder, *Fractals* (Plenum, New York, 1988).
42. A. H. England, *Complex Variable Methods in Elasticity* (Clowes, London, 1971).
43. L. D. Landau and E. M. Lifshitz, *Theory of Elasticity* (Pergamon, Oxford, 1975).
44. E. Louis, F. Guinea, F. Flores, in *Fractals in Physics*, L. Pietronero and E. Tosatti, Eds. (North-Holland, Amsterdam, 1985).
45. E. Louis and F. Guinea, *Europhys. Lett.* **3**, 871 (1987).
46. L. Fernandez, F. Guinea, E. Louis, *J. Phys. A* **21**, L301 (1988).
47. P. Meakin, G. Li, L. M. Sander, E. Louis, F. Guinea, *ibid.* **22**, 1393 (1989).
48. E. Hinrichsen, A. Hansen, S. Roux, *Europhys. Lett.* **8**, 1 (1989).
49. P. Meakin, *Crystal Prop. Prep.* **17/18**, 1 (1988).
50. B. B. Mandelbrot, in *Fractals in Physics*, L. Pietronero and E. Tosatti, Eds. (North-Holland, Amsterdam, 1986), p. 3.
51. P. Meakin, *Thin Solid Films* **151**, 165 (1987).
52. J. Ugelstad, P. C. Mork, K. H. Kaggerud, T. Ellingsen, A. Berge, *Adv. Colloid Interface Sci.* **13**, 101 (1980).
53. J. Ugelstad, P. C. Mork, A. Berge, T. Ellingsen, A. A. Kahn, in *Emulsion Polymerization*, I. Pirma, Ed. (Academic Press, New York, 1982), p. 383.
54. A. T. Skjeltorp, *Phys. Rev. Lett.* **58**, 1444 (1987).
55. _____, *J. Appl. Phys.* **57**, 3285 (1985).
56. _____, in *Time Dependent Effects in Disordered Materials*, R. Pynn and T. Riste, Eds. (NATO Advanced Study Institutes Series B167, Plenum, New York, 1987), p. 1.
57. A. T. Skjeltorp and P. Meakin, *Nature* **335**, 424 (1988).
58. Y. Termonia and P. Smith, *Macromolecules* **21**, 2184 (1988).
59. Y. Termonia and D. Walsh, *J. Mater. Sci.* **24**, 247 (1989).
60. L. R. G. Treloar, *The Physics of Rubber Elasticity* (Clarendon, Oxford, ed. 2, 1960).
61. M. R. Hestenes and E. Stiefel, *Natl. Bur. Stand. J. Res.* **49**, 409 (1952).
62. G. G. Bartrouni, A. Hansen, M. Nelkin, *Phys. Rev. Lett.* **57**, 1336 (1986).
63. A. V. Dobrodumov and L. M. El'yashevich, *Sov. Phys. Solid State* **15**, 1259 (1973).
64. Y. Termonia, P. Meakin, P. Smith, *Macromolecules* **18**, 2246 (1985).
65. _____, *ibid.* **19**, 154 (1986).
66. Y. Termonia, S. R. Allen, P. Smith, *Polymer* **27**, 1845 (1986).
67. The work described here was carried out in collaboration with F. Guinea, G. Li, E. Louis, O. Pla, L. M. Sander, A. T. Skjeltorp, Y. Termonia, and H. Yan. Figures were contributed by A. T. Skjeltorp, Y. Termonia, and H. Van Damme.

Pattern Formation During Animal Development

D. A. MELTON

At the beginning of this century, embryologists defined the central problems of developmental biology that remain today. These questions include how differentiated cells arise and form tissues and organs and how pattern is generated. In short, how does an egg give rise to an adult? In recent years, the application of molecular biology to embryological problems has led to significant advances and recast old problems in molecular and cellular terms. Although not necessarily comprehensive, this idiosyncratic review is intended to highlight selected findings and indicate where there are important gaps in our knowledge for those less than familiar with developmental biology.

IT'S NOT THE INGREDIENTS, IT'S HOW THEY'RE MIXED AND matched. A surprising and encouraging finding in recent years has been the recurring "discovery" of certain gene products in various developmental systems. Open a journal and one is likely to read that any particular gene involved in directing a given mouse cell to adopt a particular fate, after being cloned and sequenced, turns out to be related to a gene performing a similar, but not identical, function in worms, flies, or even yeast. For example, peptide growth factors, first studied for their ability to regulate cell division, now turn up in innumerable instances as signals that can tell a cell whether to become a muscle or skin cell (*1*). Similarly, fly genes involved in neurogenesis and worm genes involved in inducing vulval and gonadal lineages have both been found to encode a membrane protein with a region of amino acids related to epidermal growth factor, a gene product previously identified for its role in vertebrate epidermal differentiation (*2, 3*). Other examples include structural motifs, such as homeobox, zinc finger, helix-loop-helix, or pou domains, found in common among proteins coordinating the transcription of a set of genes and thereby directing a developmental program (*4*). These observations suggest that a few types of genes are used similarly by diverse organisms to specify cell fates during development. While differences in developmental programs between species obviously exist, these are most apparent when a developmental process is examined at the level of tissues and organs and not at the molecular level. It is perhaps self-evident that a present-day challenge for developmental biologists is to explain how relatively few types of genes (transcription factors, peptide growth factors, extracellular matrix components, cytoskeletal proteins, and so on) and mechanisms for specifying cell fates (cell-cell interactions or cytoplasmic localization among others) are used to produce such different animals. With this problem in mind, let us examine some recent findings in studies on pattern formation.

The author is in the Department of Biochemistry and Molecular Biology, Harvard University, 7 Divinity Avenue, Cambridge, MA 02138.

Regulative or Mosaic Embryos

Observations on marine invertebrates and results of experiments in which parts of embryos were cut out and studied in isolation first led embryologists to divide organisms into two classes: regulative and mosaic. In regulative embryos, parts of the embryo can be removed and the remaining cells compensate for the loss to form a normally patterned animal. Two telling examples are presented by sea urchins and salamanders. Each blastomere of a cleaving sea